

# nimblewomble: An R package for Bayesian Wombling with nimble

by Aritra Halder and Sudipto Banerjee

**Abstract** This exposition presents nimblewomble, a software package to perform wombling, or boundary analysis, using the nimble Bayesian hierarchical modeling language in the R statistical computing environment. Wombling is used widely to track regions of rapid change within the spatial reference domain. Specific functions in the package implement Gaussian process models for point-referenced spatial data followed by predictive inference on rates of change over curves using line integrals. We demonstrate model based Bayesian inference using posterior distributions featuring simple analytic forms while offering uncertainty quantification over curves.

## 1 Introduction

Detecting regions of rapid change is an important exercise in spatial data science as they harbor effects not easily explained by predictors incorporated into a spatial regression model for point-referenced spatial data. For example, environmental health scientists are often keen on identifying regions where exposure levels display rapid change or sharp gradients. Formal statistical detection of such regions can lead to data-driven discoveries of latent risk factors and other predictors that drive the rapid change in exposure surfaces. Identifying a curve that tracks such regions often guides interventions. This exercise is referred to as wombling (Womble, 1951; Gleyze et al., 2001; Banerjee, 2010). Measurement scales of the spatial data usually dictate the methods required for wombling. For areal data, boundaries delineate neighboring regions (see, e.g. Gao et al., 2023; Wu and Banerjee, 2025). Predictive inference is sought for smooth curves. We evaluate spatial gradients along a curve while assessing its candidacy for a boundary (see, e.g., Banerjee and Gelfand, 2006; Qu et al., 2021; Halder et al., 2024a), which requires specifying the smoothness of the spatial process (see, e.g. Kent, 1989; Banerjee et al., 2003).

In this software package, we are concerned with point-referenced wombling. Developing an easily accessible software that implements Bayesian wombling for use by the wider scientific community is faced with several challenges. Perhaps, the most severe being the need for two-dimensional quadrature to enable posterior inference. Our contributions here lie in the use of analytic closed forms for posteriors that require at most one-dimensional quadrature, greatly easing the computational burden and efficient Bayesian inference for hierarchical spatial models (see, e.g. Banerjee et al., 2014) via nimble (de Valpine et al., 2017) within the R (R Core Team, 2021) statistical environment.

Several R packages exist for point-referenced spatial modeling, with spBayes (Finley et al., 2007) and R-INLA (Lindgren and Rue, 2015) being more widely used. However, they do not address boundary analysis, or wombling, in any capacity. In recent years, nimble has found increased use in Bayesian modeling applications (see, e.g. Turek et al., 2016; Ponisio et al., 2020; Goldstein and de Valpine, 2022). Notable R-packages that use nimble include BayesNSGP (Risser and Turek, 2020) and nimbleEcology (Goldstein et al., 2024). The Bayesian hierarchical framework in nimblewomble is similar to spBayes. We take advantage of the one line call and execute feature of nimble to develop Markov Chain Monte Carlo (MCMC) algorithms for fitting Gaussian process (GPs). This makes the underlying code for nimblewomble easily accessible and customizable for wider use.

We demonstrate our developments using the Matérn class of covariance kernels (see, e.g., Abramowitz et al., 1988). They are a popular choice in the literature for GPs (see, e.g., Rasmussen and Williams, 2005). They feature a fractal parameter that provides explicit control over process smoothness. Our package offers three choices for the fractal parameter allowing for flexible process specification. Gradient estimation is done on a grid. We show an example of generating an equally spaced grid. Users can also specify a grid of their choice. Wombling requires a curve, we use contours for that purpose. We demonstrate the procedure for obtaining contours using the raster package. Alternatively, a curve of choice can also be used. Our vignettes show an example that uses the locator() function. The user annotates points on the interpolated surface and a smooth Bézier curve is generated for use. Finally, posterior samples from models in spBayes can also be used for wombling with nimblewomble. The same kernel needs to be used in both packages to ensure valid inference.

The nimblewomble package is available for download on the Comprehensive R Archive Network (CRAN) at <https://cran.rstudio.com/web/packages/nimblewomble/>. It contains functions that are required to perform wombling. These functions are described in Table 1. Broadly, they can be classified into four categories: covariance kernels, model fitting, inference on rates of change and line integrals and graphical displays. All functions, with the exception of plotting, are scripted as nimbleFunctions with wrapper functions that are callable through R. This enables fast execution using their compiled

Function	Purpose	Description
materncov1	covariance kernel	Matérn covariance with $\nu = \frac{3}{2}, \frac{5}{2}$ and $\infty$ (squared exponential kernel)
materncov2		
gaussian		
gp_fit	model fitting	Fits a Gaussian Process with non-informative priors. Produces posterior samples for $\theta$
zbeta_samples	model fitting	Posterior samples for $Z(s)$ and $\beta$
sprates	inference	Posterior samples for $\partial Z(s)$ and $\partial^2 Z(s)$
spwombling	inference	Posterior samples for $\Gamma(C)$
sp_ggplot	plotting	Interpolated spatial surface plots

**Table 1:** Summary of functions that are required for wombling using `nimblewomble`.

C++ counterparts. We generate spatial graphics using `ggplot2` (Wickham, 2011) and `MBA` (Finley, 2024). Other helper functions within the package serve specific computational purposes, for example, the incomplete Gamma integral is computed by `gamma_int`. They are primarily for internal use and hence, not included in the table. In the following sections we describe the methodological details briefly and provide an overview of the functions within `nimblewomble` with worked out examples to demonstrate the workflow using a spatial transcriptomics dataset.

## 2 Spatial Processes for Rates of Change

We consider  $\{Y(s) : s \in \mathcal{S} \subseteq \mathbb{R}^2\}$  to be a univariate weakly stationary random field with zero mean and a positive definite covariance  $K(s, s') = \text{Cov}(Y(s), Y(s'))$  for locations  $s, s' \in \mathbb{R}^2$ . Mean square smoothness (see, e.g., Stein, 1999) at an arbitrary location  $s_0$  requires  $Y(s_0 + hu) = Y(s_0) + hu^\top \partial Y(s_0) + h^2 u^{\otimes 2 \top} \partial^{\otimes 2} Y(s_0) + o(h^3 \|u\|^3)$ , where  $u = (u_1, u_2)^\top \in \mathbb{R}^2$  is an arbitrary vector of directions,  $\partial$  is the gradient operator,  $\partial Y(s_0) = \left( \frac{\partial}{\partial s_x} Y(s_0), \frac{\partial}{\partial s_y} Y(s_0) \right)^\top = (\partial_x Y(s_0), \partial_y Y(s_0))^\top$ ,  $\otimes$  is the Kronecker vector product. Hence,  $u^{\otimes 2} = (u_1^2, u_1 u_2, u_2 u_1, u_2^2)^\top$  and  $\partial^{\otimes 2} = \partial \otimes \partial$ . Note that  $\partial^{\otimes 2} Y(s_0)$  is the vectorized Hessian. The processes  $\partial Y(s_0)$  and  $\partial^{\otimes 2} Y(s_0)$  govern rates of change in  $Y(s_0)$ . The *gradient* or, first order rate of change, is captured by  $\partial Y(s_0)$  while, *curvature* is captured by  $\partial^{\otimes 2} Y(s_0)$ . *Mean square differentiability* (see Banerjee and Gelfand, 2003) of the first and second order for  $Y(s_0)$  guarantees that  $u^\top \partial Y(s_0)$  and  $(u \otimes v)^\top \partial^{\otimes 2} Y(s_0)$  are well-defined respectively, for any set of direction vectors  $u, v \in \mathbb{R}^2$ . We note that the entries of  $\partial^{\otimes 2} Y(s_0)$  contain duplicates, both  $\frac{\partial^2}{\partial s_x \partial s_y} Y(s_0)$  and  $\frac{\partial^2}{\partial s_y \partial s_x} Y(s_0)$  are included. To avoid singularities that arise from duplication, we work with  $\tilde{\partial}^{\otimes 2} Y(s_0) = \left( \frac{\partial^2}{\partial s_x^2} Y(s_0), \frac{\partial^2}{\partial s_x \partial s_y} Y(s_0), \frac{\partial^2}{\partial s_y^2} Y(s_0) \right)^\top$  comprised of only unique derivatives.

Statistical inference is devised for the joint process,  $\mathcal{L}^* Y(s) = \left( Y(s), \partial Y(s)^\top, \tilde{\partial}^{\otimes 2} Y(s)^\top \right)^\top$ . Validity of the inference is considered at length in Banerjee et al. (2003); Halder et al. (2024a). The process  $\mathcal{L}^* Y(s)$  is also weakly stationary with a cross-covariance matrix,

$$\mathbf{V}_{\mathcal{L}^*}(\Delta) = \begin{pmatrix} K(\Delta) & \partial K(\Delta)^\top & \tilde{\partial}^2 K(\Delta)^\top \\ -\partial K(\Delta) & -\partial^2 K(\Delta) & -\tilde{\partial}^3 K(\Delta)^\top \\ \tilde{\partial}^2 K(\Delta) & \tilde{\partial}^3 K(\Delta) & \tilde{\partial}^4 K(\Delta) \end{pmatrix}, \quad (1)$$

where  $\Delta = s - s'$ ,  $\partial K(\Delta)$  is a  $2 \times 1$  vector of gradients,  $\tilde{\partial}^2 K(\Delta)$  is a  $3 \times 1$  vector of unique curvatures,  $\tilde{\partial}^3 K(\Delta)$  is a  $3 \times 2$  matrix of third derivatives,  $\partial^2 K(\Delta)$  is the  $2 \times 2$  Hessian and  $\tilde{\partial}^4 K(\Delta)$  is a  $3 \times 3$  matrix of fourth order derivatives. Evidently, for  $\mathbf{V}_{\mathcal{L}^*}(\Delta)$  in eq. (1) to be valid all entries need to be well-defined.

Let  $Y(s) \sim GP(0, K(\cdot; \theta))$  denote a Gaussian process (GP) where  $K(\Delta; \theta) = \text{Cov}(Y(s), Y(s'))$  with process parameters  $\theta = \{\sigma^2, \phi\}$ . We will denote  $K(\Delta; \theta) = K(\Delta)$  to ease notation. The covariance function satisfies  $\sum_{i=1}^N \sum_{j=1}^N a_i a_j K(\Delta_{ij}) > 0$  for any collection of coordinates  $\{s_i : i = 1, \dots, N\}$ . Under isotropy we have  $K(\Delta) = \tilde{K}(\|\Delta\|)$ . Let  $\mathbf{y} = (y(s_1), \dots, y(s_N))^\top$  be the observed realization over  $\mathcal{S}$ ,  $\Sigma_{\mathbf{y}}$  be the  $N \times N$  covariance matrix with entries  $K(s_i, s_j)$ ,  $i, j = 1, \dots, N$  and  $s_0$  an arbitrary location of interest. The joint distribution is as follows:

$$\mathbf{y}, \partial Y(s_0), \bar{\partial}^2 Y(s_0) | \boldsymbol{\theta} \sim \mathcal{N}_{N+5} \left( \mathbf{0}_{N+5}, \begin{pmatrix} \boldsymbol{\Sigma}_{\mathbf{y}} & \mathbf{K}_1 & \mathbf{K}_2 \\ -\mathbf{K}_1^\top & -\bar{\partial}^2 K(\mathbf{0}) & -\bar{\partial}^3 K(\mathbf{0})^\top \\ \mathbf{K}_2^\top & \bar{\partial}^3 K(\mathbf{0}) & \bar{\partial}^4 K(\mathbf{0}) \end{pmatrix} \right), \quad (2)$$

where,  $\mathcal{N}_d$  denotes the  $d$ -variate Gaussian distribution,  $\mathbf{K}_1 = (\partial K(\delta_{10})^\top, \dots, \partial K(\delta_{N0})^\top)^\top$ ,  $\mathbf{K}_2 = (\bar{\partial}^2 K(\delta_{10})^\top, \dots, \bar{\partial}^2 K(\delta_{N0})^\top)^\top$  and  $\delta_{i0} = s_i - s_0$ ,  $i = 1, \dots, N$ . The resulting posterior predictive distribution for rates of change at  $s_0$  is  $P(\partial Y(s_0), \bar{\partial}^2 Y(s_0) | \mathbf{y}) = \int P(\partial Y(s_0), \bar{\partial}^2 Y(s_0) | \mathbf{y}, \boldsymbol{\theta}) P(\boldsymbol{\theta} | \mathbf{y}) d\boldsymbol{\theta}$ . Posterior sampling proceeds in a one-for-one fashion corresponding to posterior samples of  $\boldsymbol{\theta}$ . From eq. (2) the resulting full conditional distribution is obtained as follows:

$$\begin{pmatrix} \partial Y(s_0) \\ \bar{\partial}^2 Y(s_0) \end{pmatrix} | \mathbf{y} \sim \mathcal{N}_5 \left( - \begin{pmatrix} \mathbf{K}_1 \\ \mathbf{K}_2 \end{pmatrix}^\top \boldsymbol{\Sigma}_{\mathbf{y}}^{-1} \mathbf{y}, \begin{pmatrix} -\bar{\partial}^2 K(\mathbf{0}) & -\bar{\partial}^3 K(\mathbf{0})^\top \\ \bar{\partial}^3 K(\mathbf{0}) & \bar{\partial}^4 K(\mathbf{0}) \end{pmatrix} - \begin{pmatrix} \mathbf{K}_1 \\ \mathbf{K}_2 \end{pmatrix}^\top \boldsymbol{\Sigma}_{\mathbf{y}}^{-1} \begin{pmatrix} \mathbf{K}_1 \\ \mathbf{K}_2 \end{pmatrix} \right). \quad (3)$$

We use the Matérn class of kernels,  $K(\|\Delta\|, \boldsymbol{\theta}) = \sigma^2 \Gamma(\nu)^{-1} 2^{1-\nu} (\sqrt{2\nu\phi\|\Delta\|})^\nu K_\nu(\sqrt{2\nu\phi\|\Delta\|})$ , where  $K_\nu(\cdot)$  is the modified Bessel function of the second kind (Abramowitz et al., 1988) featuring a fractal parameter  $\nu$  that controls process smoothness, a spatial range parameter  $\phi$  and an overall variance parameter  $\sigma^2$ .

### 3 Spatial Wombling

The wombling exercise seeks posterior predictive inference on line integrals

$$\Gamma(C) = \left( \int_C \mathbf{u}^\top \partial Y(s) ds, \int_C \mathbf{u}^{\otimes 2 \top} \bar{\partial}^2 Y(s) ds \right)^\top, \quad (4)$$

where  $C$  is a curve of interest to the investigator. Average wombling measures are defined as  $\bar{\Gamma}(C) = \Gamma(C)/\ell(C)$ , where  $\ell$  is the arc-length measure. For closed curves we replace  $\int$  with  $\oint$  in eq. (4). The choice of direction is crucial when measuring rates of change. The curve  $C$  typically tracks a region of rapid change in the reference domain and hence, the direction normal to  $C$  is naturally of interest. We denote the normal to  $C$  at  $s$  by  $\mathbf{n}(s)$  and set  $\mathbf{u} = \mathbf{n}(s)$  in the line integrals of eq. (4). The curve  $C$  is deemed to be a *wombling boundary* if any entry of  $\Gamma(C)$  is large. Focusing on the choices for  $C$ , not all curves ensure the existence of  $\mathbf{n}(s)$  at every  $s$ . Parametric smooth curves offer some respite in that regard. We work with  $C = \{s(t) = (s_1(t), s_2(t)) : t \in I \subset \mathbb{R}\}$ . As  $t$  varies over  $I$ ,  $s(t)$  traces out  $C$ . We assume  $\|s'(t)\| \neq 0$  which ensures  $\mathbf{n}(s) = \|s'(t)\|^{-1} (s_2'(t), -s_1'(t))^\top$  is well-defined.

The arc-length,  $\ell(C) = \int_I \|s'(t)\| dt$ . For parametric curves  $\Gamma(C)$  can be expressed as,  $\Gamma(C) = \left( \int_I \mathbf{n}(s(t))^\top \partial Y(s(t)) \|s'(t)\| dt, \int_I \mathbf{n}(s(t))^{\otimes 2 \top} \bar{\partial}^2 Y(s(t)) \|s'(t)\| dt \right)^\top$ . Let  $I = [0, t^*]$ , and the curve traced out over  $I$  be denoted as  $C_{t^*}$ . Statistical inference for  $\Gamma(C_{t^*})$  follows from  $\partial Y(s)$  and  $\bar{\partial}^2 Y(s)$  being GPs, as seen in eq. (3),  $\Gamma(C_{t^*}) \sim \mathcal{N}_2(\mathbf{0}_2, \mathbf{K}_\Gamma(t^*, t^*))$ , where  $\mathbf{K}_\Gamma(t^*, t^*)$  is a  $2 \times 2$  matrix with entries

$$k_{ij}(t^*, t^*) = (-1)^i \int_0^{t^*} \int_0^{t^*} \mathbf{a}_i(t_1)^\top \partial^{i+j} K(\Delta(t_1, t_2)) \mathbf{a}_j(t_2) \|s'(t_1)\| \|s'(t_2)\| dt_1 dt_2, \quad (5)$$

where  $\mathbf{a}_1(t) = \mathbf{n}(s(t))$ ,  $\mathbf{a}_2(t) = \mathcal{E}_2 \mathbf{n}(s(t))^{\otimes 2}$ , with  $\mathcal{E}_2 = \begin{pmatrix} 1 & & \\ & 1 & \\ & & 1 \end{pmatrix}$  being an elimination matrix and  $\Delta(t_1, t_2) = s_2(t) - s_1(t)$  for  $i, j = 1, 2$ . Predictive inference on  $\Gamma(C)$  requires

$$\mathbf{y}, \Gamma(C_{t^*}) | \boldsymbol{\theta} \sim \mathcal{N}_{N+2} \left( \mathbf{0}_{N+2}, \begin{pmatrix} \boldsymbol{\Sigma}_{\mathbf{y}} & \mathcal{G}_\Gamma(t^*)^\top \\ \mathcal{G}_\Gamma(t^*) & \mathbf{K}_\Gamma(t^*, t^*) \end{pmatrix} \right), \quad (6)$$

where  $\mathcal{G}_\Gamma(t^*)^\top = \begin{pmatrix} \gamma_1(t^*)^\top \\ \vdots \\ \gamma_N(t^*)^\top \end{pmatrix}$  is an  $N \times 2$  matrix with entries

$$\gamma_i(t^*) = \left( \int_0^{t^*} \mathbf{n}(s(t))^\top \partial K(\Delta_j(t)) \|s'(t)\| dt, \int_0^{t^*} \mathbf{n}(s(t))^{\otimes 2 \top} \bar{\partial}^2 K(\Delta_j(t)) \|s'(t)\| dt \right)^\top, \quad (7)$$

where  $\Delta_j(t) = s(t) - s_j$ . Posterior predictive inference proceeds one-for-one (similar to eq. (3)) using  $\Gamma(C_{t^*}) | \mathbf{y} \sim \mathcal{N}_2(-\mathcal{G}_\Gamma(t^*) \boldsymbol{\Sigma}_{\mathbf{y}}^{-1} \mathbf{y}, \mathbf{K}_\Gamma(t^*, t^*) - \mathcal{G}_\Gamma(t^*) \boldsymbol{\Sigma}_{\mathbf{y}}^{-1} \mathcal{G}_\Gamma(t^*)^\top)$ .

In practice, modern computing environments store curves as a set of points. As a result, it suffices to demonstrate wombling for rectilinear approximations to smooth curves where predictive inference is performed iteratively on segments. We show the inference for one generic segment. Let  $C = \{s(t_0), s(t_1), \dots, s(t_{n_p})\}$ , then the  $i$ -th segment,  $C_i = \{s(t) = s(t_{i-1}) + t\mathbf{u}_i : t \in [0, t_i]\}$ ,

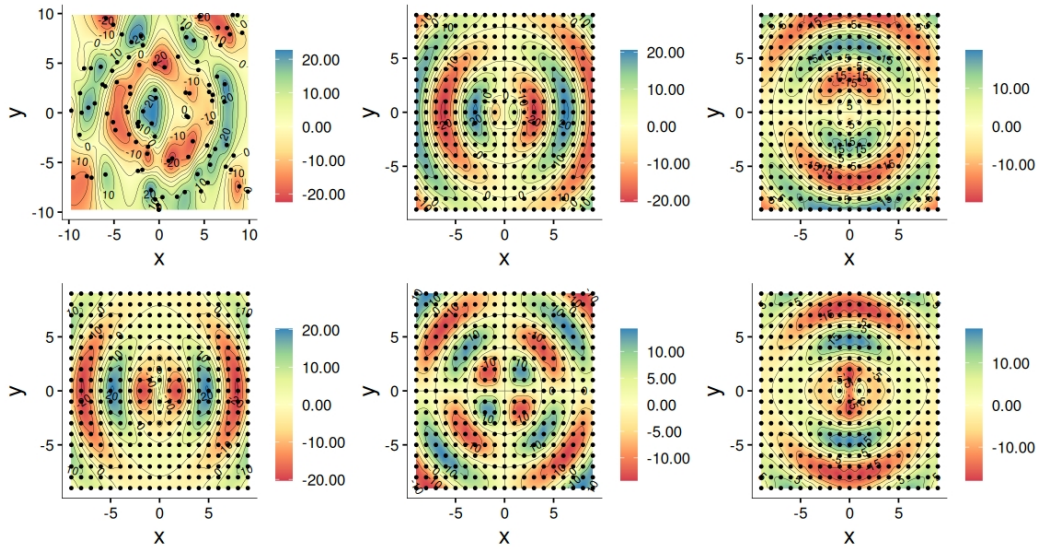


**Figure 1:** Patterned data used for experiments. Top row: (left) simulated process (middle)  $\partial_x$  (right)  $\partial_y$ . Bottom row: (left)  $\partial_{xx}^2$  (middle)  $\partial_{xy}^2$  (right)  $\partial_{yy}^2$ . The grid used is overlaid on the plots.

$t_i = \|s(t_i) - s(t_{i-1})\|$  and  $u_i = t_i^{-1}(s(t_i) - s(t_{i-1}))$ . Clearly,  $\|u_i\| = 1$ ,  $\|s'(t)\| = 1$  and the normal to  $C_{t_i}$  is  $u_i^\perp = (u_{i2}, -u_{i1})^\top$ . For predictive inference on  $\Gamma(C_{t_i})$ , note that we need  $\Delta(t_1, t_2) = (t_2 - t_1)u_i$  in eq. (5) and  $\Delta_j(t) = \Delta_{i-1,j} + tu_i = (s_{i-1} - s_j) + tu_{i-1}$  in eq. (7).

### Wombling with Closed Forms

We acknowledge that eq. (5) requires 2-dimensional quadrature which is computationally expensive to evaluate. We work with the Matérn kernel for which closed form analytic expressions exist for the entries of  $\mathbf{K}_\Gamma(t^*, t^*)$  improving on Banerjee and Gelfand (2006); Halder et al. (2024a) (see Theorems 1 & 2 in the Supplement). The benefits are reduced computation time and ease of implementation. Our R-package, `nimblewomble` features Matérn kernels with  $\nu = \frac{3}{2}, \frac{5}{2}$  and  $\infty$  (squared exponential).

## 4 Bayesian Hierarchical Models

A Bayesian hierarchical model is specified as follows:

$$Y(s) = \mu(s, \beta) + Z(s) + \epsilon(s), \tag{8}$$

where  $\mu(s, \beta) = x(s)^\top \beta$ ,  $Z(s) \sim GP(0, K(\cdot; \sigma^2, \phi))$  and  $\epsilon(s)$  is a white noise process (i.e.,  $\epsilon(s_i) \stackrel{iid}{\sim} N(0, \tau^2)$  over any finite collection of locations). The process parameters are  $\theta = \{\sigma^2, \phi, \tau^2\}$ . Predictive inference for  $\mathcal{L}^*Z(s)$  evaluates  $P(\partial Z(s)^\top, \bar{\partial}^2 Z(s)^\top | \mathcal{Y}) = \int P(\partial Z(s)^\top, \bar{\partial}^2 Z(s)^\top | \mathcal{Z}, \theta) P(\mathcal{Z} | \mathcal{Y}, \theta) P(\theta | \mathcal{Y}) d\theta d\mathcal{Z}$ . Similarly for the wombling measures,  $P(\Gamma_{\mathcal{Z}}(C_r) | \mathcal{Y}) = \int P(\Gamma_{\mathcal{Z}}(C_r) | \mathcal{Z}, \theta) P(\mathcal{Z} | \mathcal{Y}, \theta) P(\theta | \mathcal{Y}) d\theta d\mathcal{Z}$ . A customary *collapsed* posterior (see, e.g. Finley et al., 2019) for  $\theta$  is specified as follows:

$$P(\theta | \mathcal{Y}) \propto U(\phi | a_\phi, b_\phi) \times IG(\sigma^2 | a_\sigma, b_\sigma) \times IG(\tau^2 | a_\tau, b_\tau) \times N_N(\mathcal{Y} | \mathbf{X}\beta, \Sigma + \tau^2 \mathbf{I}_N), \tag{9}$$

where  $\Sigma = \sigma^2 \mathbf{R}_{\mathcal{Z}}(\phi)$ , with  $\mathbf{R}_{\mathcal{Z}}(\phi)$  being the correlation matrix corresponding to  $K(\cdot; \sigma^2, \phi)$ ,  $U(\cdot | \cdot)$  is the uniform distribution and  $IG(\cdot | \cdot)$  is the inverse-gamma distribution. Hyper-parameters are chosen such that a non-informative prior is specified on  $\theta$ . Posterior samples for  $\mathcal{Z}$  and  $\beta$  are generated one-for-one corresponding to posterior samples of  $\theta$  using a Gibbs sampling scheme.

Posterior sampling in eq. (9) is straightforward in `nimbleCode` as seen in the code for `gp_model1` below, which forms the core of our `gp_fit` function (see Table 1). We take advantage of the *one-line call and execute* feature of `nimble` using the `buildMCMC` and `runMCMC` functions to obtain posterior samples from eq. (9) thereby, fitting eq. (8).

```
#####
# Collapsed Metropolis-Hastings #
```

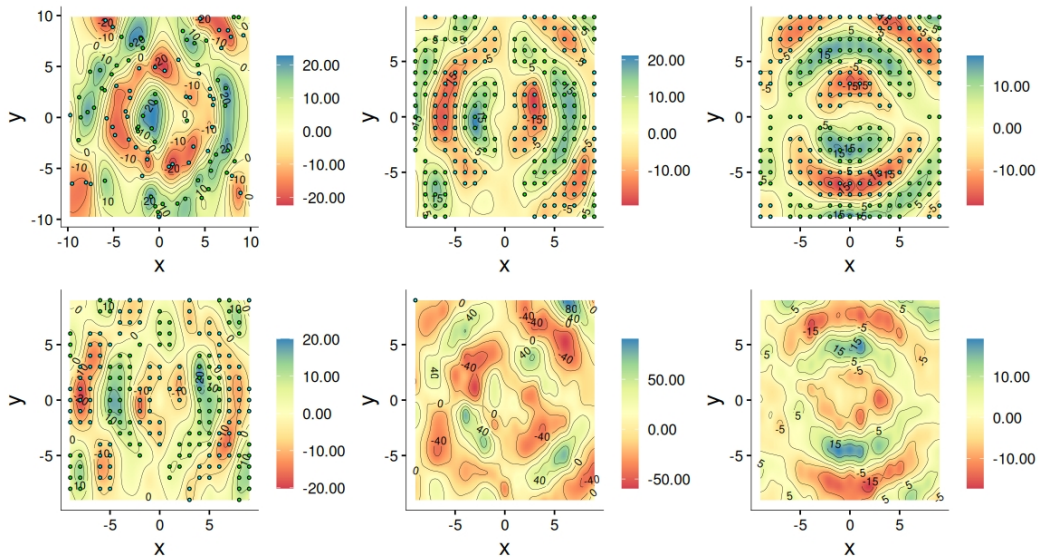


Figure 2: Estimated patterns with highlighted significant locations: positive (green) negative (cyan).

```
# for covariance parameters #
#####

gp_model <- nimbleCode({
  # Priors #
  phi ~ dunif(0, 10)
  sigma2 ~ dinvgamma(shape = 1, rate = 1)
  tau2 ~ dinvgamma(shape = 2, rate = 1)

  # Initialization #
  mu[1:N] <- zeros[1:N] # vector of 0s
  cov[1:N, 1:N] <- kernel(dists[1:N, 1:N], phi, sigma2, tau2)

  # Likelihood #
  y[1:N] ~ dmnorm(mu[1:N], cov = cov[1:N, 1:N])
})
```

Note that for different choices kernel is replaced with the corresponding kernel choice in Table 1.

## 5 Workflow of nimblewomble

We detail the workflow for `nimblewomble` using simulated data. We produce data using patterns that yield closed form expressions for rates of change. This helps calibrate the predictive performance of `nimblewomble`. We generate  $N = 100$  observations over  $[-10, 10] \times [-10, 10] \subseteq \mathbb{R}^2$  arising from,  $y(s) \sim \mathcal{N}_1(\mu_0(s) = 20 \sin \|s\|, \tau^2)$ . We set  $\tau^2 = 1$ . Here, the true values of gradients are available in closed-form. For example,  $\partial_x \mu_0(s_G) = 20 \cos \|s_G\| s_{x,G} \|s_G\|^{-1}$ , where  $s_G = (s_{x,G}, s_{y,G})$  lies on a grid overlaid on the domain of reference (in this case:  $[-10, 10] \times [-10, 10]$ ). Other gradient and curvature processes are computed similarly by differentiating  $\mu_0(s)$ . Running the following code generates the simulated data and produces plots in Figure 1.

```
set.seed(1)
# Generating Simulated Data
N = 1e2
tau = 1
coords = matrix(runif(2 * N, -10, 10), ncol = 2); colnames(coords) = c("x", "y")
y = rnorm(N, mean = 20 * sin(sqrt(coords[, 1]^2 + coords[, 2]^2)), sd = tau)

# Create equally spaced grid of points
```

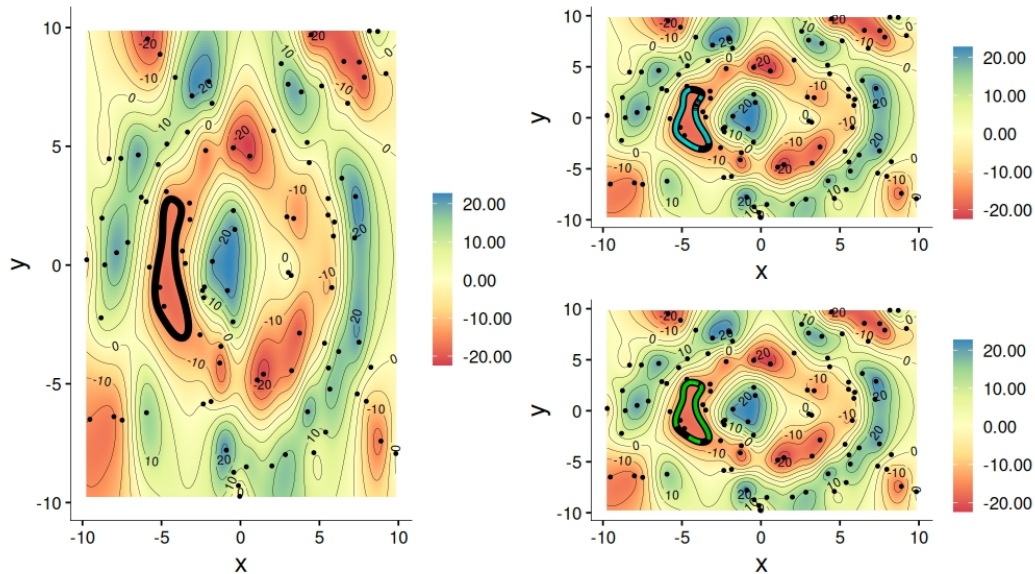


**Figure 3:** (Left) Curve chosen for wombling, (Right-top) gradient wombling measure for line segments, (Right-bottom) curvature wombling measure for line segments. Significant segments are highlighted: positive (green) negative (cyan).

```

xsplit = ysplit = seq(-10, 10, by = 1)[-c(1, 21)]
grid = as.matrix(expand.grid(xsplit, ysplit), ncol = 2)
colnames(grid) = c("x", "y")

#####
# Process for True Rates of Change #
#####
# Gradient along x
true_sx = round(20 * cos(sqrt(grid[,1]^2 + grid[,2]^2)) *
                grid[,1]/sqrt(grid[,1]^2 + grid[,2]^2), 3)
# Gradient along y
true_sy = round(20 * cos(sqrt(grid[,1]^2 + grid[,2]^2)) *
                grid[,2]/sqrt(grid[,1]^2 + grid[,2]^2), 3)
# Plotting
sp_ggplot(data_frame = data.frame(coords, z = y))
sp_ggplot(data_frame = data.frame(grid[-which(is.nan(true_sx)), ],
                                z = true_sx[-which(is.nan(true_sx))]))

```

We fit the model in eq. (8) using `gp_fit` using a Matérn kernel with  $\nu = \frac{5}{2}$  to the simulated data. This allows for inference on gradients and curvatures. Running the code below first generates posterior samples of  $\theta$  from eq. (9) followed by posterior samples for  $Z(s)$  and  $\beta$  one-for-one  $\theta$ . The `mc_sp` object is a list comprised of (a) MCMC samples for  $\theta$  stored in `mc_sp$mcmc` and (b) the estimates: median and 95% confidence intervals (CIs) stored in `mc_sp$estimates`. Posterior samples for  $Z(s)$  and  $\beta$  are obtained using `zbeta_samples` as seen below. The model object contains samples for  $\theta$ ,  $Z$  and  $\beta$ .

```

require(nimble)
require(nimblewomble)

#####
# Fit a Gaussian Process #
#####
# Posterior samples for theta
mc_sp = gp_fit(coords = coords, y = y, kernel = "matern2")
# Posterior samples for Z(s) and beta
model = zbeta_samples(y = y, coords = coords,
                     model = mc_sp$mcmc,
                     kernel = "matern2")

```

Next, we estimate gradients and curvatures using the posterior samples of  $\phi$ ,  $\sigma^2$  and  $Z$  using the

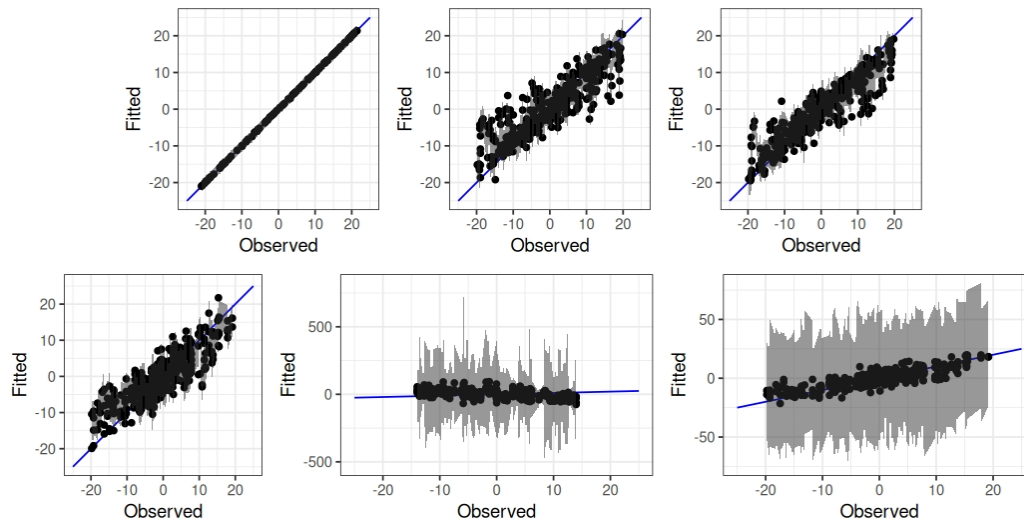


**Figure 4:** Diagnostics assessing quality of fit using observed vs. fitted values for (Top) (left) response (center)  $\partial_x$  (right)  $\partial_y$  (Bottom) (left)  $\partial_{xx}^2$  (center)  $\partial_{xy}^2$  (right)  $\partial_{yy}^2$  with 95% confidence bands.

sprates function. The output stored in `gradients` contains posterior samples and estimates: median and 95% CIs for gradients and curvatures required to produce the plots in Figure 2. Posterior sampling is done one-for-one for samples of  $\phi$ ,  $\sigma^2$  and  $\mathcal{Z}$ .

```
#####
# Rates of Change #
#####
gradients = sprates(grid = grid,
                    coords = coords,
                    model = model,
                    kernel = "matern2")
# Plot estimated gradients along x
sp_ggplot(data_frame = data.frame(grid,
                                   z = gradients$estimate.sx["50%"],
                                   sig = gradients$estimate.sx$sig))
```

The wombling exercise requires a curve. The easiest choice of curves are contours. In **R**, a rasterized surface using the `raster` package can be used to lift contours from the interpolated surface (as seen in the plot Figure 1 top row left). The code below shows an example. The curve is shown in Figure 3.

```
require(MBA)
require(raster)
# Rasterized Surface
surf <- raster(mba.surf(data.frame(cbind(coords, z = y)),
                      no.X = 300,
                      no.Y = 300,
                      h = 5,
                      m = 2,
                      extend = TRUE, sp = FALSE)$xyz.est)
# convert raster surface to contours
x = rasterToContour(surf, nlevel = 10)

x.levels <- as.numeric(as.character(x$level))
# Curve from a region of relatively low values
curves.pm.subset = subset(x, level == -15)
```

Wombling is performed on this curve using the `spwombling` function. Posterior samples of  $\Gamma(C)$ , where  $C$  is the chosen curve, are generated one-for-one  $\sigma^2$ ,  $\phi$  and  $\mathcal{Z}$ . The code below provides an example. The output is comprised of posterior samples (`wm$wm.mcmc`) of  $\Gamma(C)$  and estimates: median and 95% CI (`wm$estimate.wm`). It also produces the plots in Figure 3.

```
require(patchwork)
```

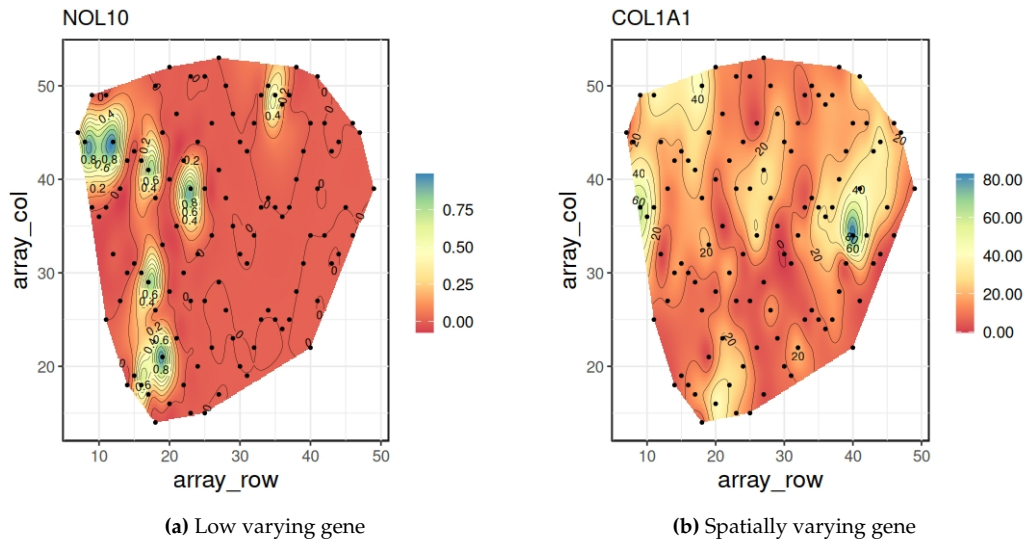


**Figure 5:** Surfaces for gene expression of a low varying gene and spatially varying gene.

```
#####
# Wombling #
#####
wm = spwombling(coords = coords,
                curve = curve,
                model = model,
                kernel = "matern2")
# Total wombling measure for gradient
colSums(wm$estimate.wm.1[, -4])
# Total wombling measure for curvature
colSums(wm$estimate.wm.2[, -4])

# Color code line segments based on significance
# of gradient based wombling measure
col.pts.1 = sapply(wm$estimate.wm.1$sig, function(x){
  if(x == 1) return("green")
  else if(x == -1) return("cyan")
  else return(NA)
})
# Color code line segments based on significance
# of curvature based wombling measure
col.pts.2 = sapply(wm$estimate.wm.2$sig, function(x){
  if(x == 1) return("green")
  else if(x == -1) return("cyan")
  else return(NA)
})
#####
# Plots for Wombling #
#####
p1 = sp_ggplot(data_frame = data.frame(coords, y))
# Plot in Figure 3 (left)
p2 = p1 + geom_path(curve, mapping = aes(x, y), linewidth = 2)
# Plot in Figure 3 (top-right): gradient
p3 = p1 + geom_path(curve, mapping = aes(x, y), linewidth = 2) +
  geom_path(curve, mapping = aes(x, y),
            colour = c(col.pts.1, NA), linewidth = 1, na.rm = TRUE)
# Plot in Figure 3 (bottom-right): curvature
p4 = p1 + geom_path(curve, mapping = aes(x, y), linewidth = 2) +
  geom_path(curve, mapping = aes(x, y),
            colour = c(col.pts.2, NA), linewidth = 1, na.rm = TRUE)
```



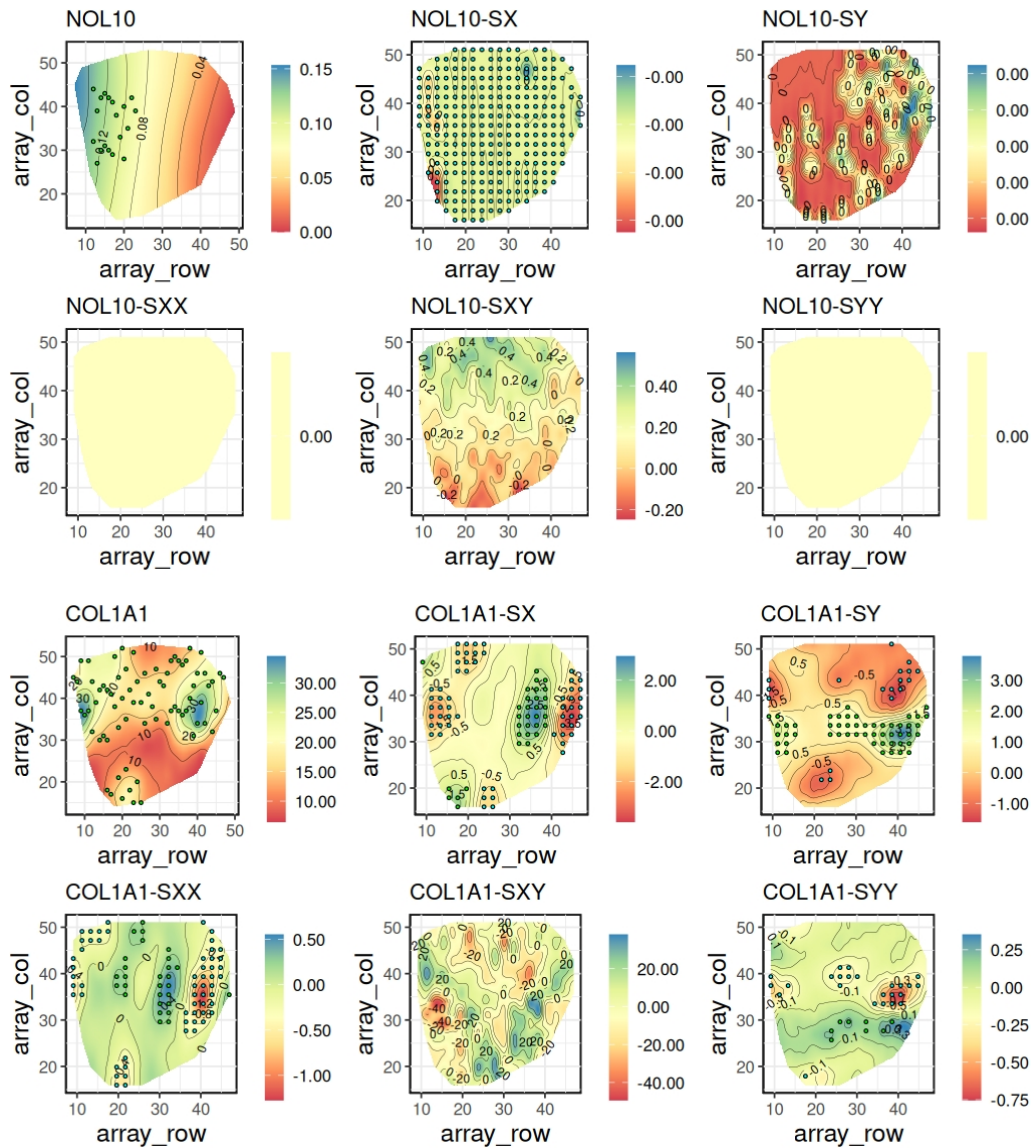


**Figure 6:** Plots comparing gradients for the two genes. First two rows are for the low varying gene. Bottom two rows are for the high varying gene. Significant grid locations are highlighted.

`p2 + (p3/p4) # generates Fig. 3`

We conclude the workflow with some brief comments on assessing the quality of fit. The default setting of `gp_fit` generates 10,000 posterior samples, with a 5,000 burn-in. The model fit was satisfactory:  $\widehat{\tau}^2 = 0.384$  (0.145, 1.433) containing the true value of 1,  $\widehat{\sigma}^2 = 344.680$  (194.292, 687.247) and  $\widehat{\phi} = 0.380$  (0.302, 0.489) which can be obtained from `mc_sp$estimates`. We achieved  $\approx 96\%$  coverage for the estimated rates of change and wobbling measures at the line segment level. For the wobbling measure,  $\widehat{\Gamma}(C) = (-108.765, 154.565)^T$ , with 95% CIs being  $(-182.098, -36.290)$  and  $(69.053, 241.664)$  respectively, containing the true values  $\Gamma(C) = (-131.149, 144.010)^T$ . They are obtained from `wm$estimate.wm.1` and `wm$estimate.wm.2`. The curve  $C$  forms a *wobbling boundary*. Figure 4 shows further diagnostics for model fit.

## 6 nimblewomble in Action: Spatial Omics

We demonstrate the workflow of `nimblewomble` on a spatial omics dataset which is also supplied with the package. The data is an abridged version of what can be found in the Gene Expression Omnibus (accession number [GSE144239](https://www.ncbi.nlm.nih.gov/geo/query/acc.cgi?acc=GSE144239)) (see, e.g., Ji et al., 2020). It consists of gene expressions with tumor sampling locations for human squamous cell carcinoma, commonly known as *skin cancer*. Detecting

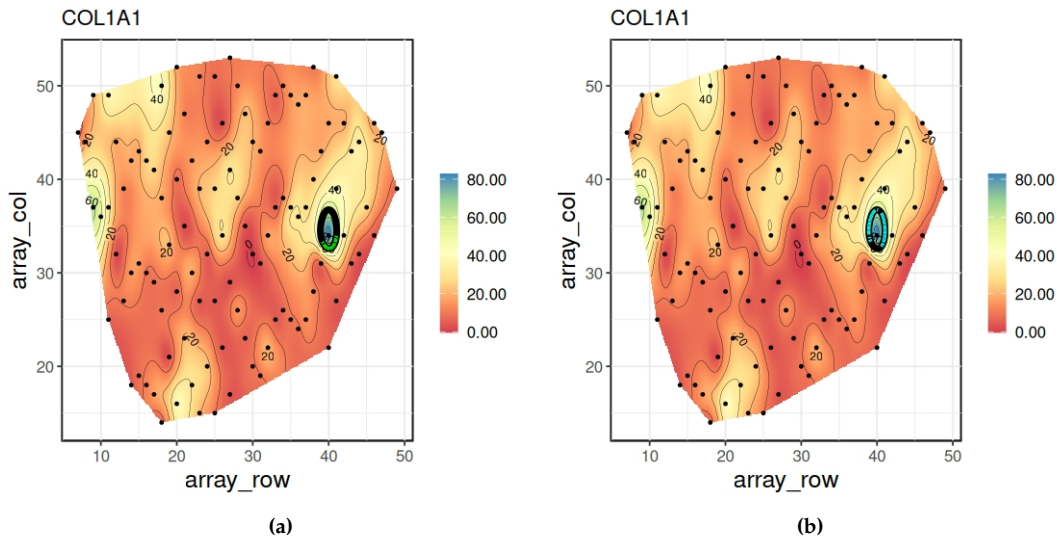


**Figure 7:** Line segment level inference for (a) gradient and (b) curvature wombling measures.

variation in gene expression is key to identifying genetic pathways specific to the cancer-type. This has led to large body of research that focuses on identifying spatially varying genes (SVGs) (see, e.g., Svensson et al., 2018; Sun et al., 2020; Weber et al., 2023; Chen et al., 2024). We use rates of change to investigate differences between a SVG (COL1A1) and a low variance gene (NOL10).

```
#####
# Load the Data #
#####
load("genes.RData")
coords = genes[, 1:2]
y = genes[, 4]; gene = "COL1A1"
N = length(y)
# Make a spatial plot of the genetic expression
sp_ggplot(data_frame = data.frame(coords, z = y),
          extend = FALSE, title = gene)
```

The data can be loaded into the **R** console by running the above code. Running `sp_ggplot` produces an interpolated spatial plot of the raw gene expression counts as seen in Figure 5b. Using `genes[, 3]` and running the same code produces Figure 5a. Comparing the ranges for the two plots the differences in expression is immediate.

We begin by fitting the GP model to individual gene expressions using `gp_fit`. For COL1A1:  $\hat{\tau}^2 = 120.667$  (68.168, 198.105),  $\hat{\sigma}^2 = 225.652$  (78.750, 529.670);  $\hat{\phi} = 0.118$  (0.015, 0.217), while for NOL10:  $\hat{\tau}^2 = 0.081$  (0.063, 0.017),  $\hat{\sigma}^2 = 0.676$  (0.191, 6.211);  $\hat{\phi} = 0.004$  (0.001, 0.016). These can be accessed by running `$estimates` on the object that stores `gp_fit`. We use a Matérn kernel with  $\nu = \frac{5}{2}$ .

Following up with gradient and curvature estimation using `sprates`, the resulting plots are shown in Figure 6. The top two rows are for NOL10, while the bottom two rows are for COL1A1 which is an SVG. In each set, the first plot shows the fitted process followed by the gradients:  $-SX$ ,  $-SY$  and the curvatures:  $-SXX$ ,  $-SXY$  and  $-SYY$ . Comparing the magnitude of corresponding gradients and curvatures we see more significant grid locations show up for rates of change for the SVG as compared to the NOL10. This provides a more detailed picture of the manifestation of variation in the SVG rather than comparing estimates of overall variance.

Finally, we pick a curve within the expression surface of COL1A1 that tracks a region of high expression (see Figure 5b) and performed wombling using `spwombling`. The results for the gradient based wombling measure and the curvature based wombling measure are shown in Figure 7a and Figure 7b respectively;  $\hat{\Gamma}(C) = (18.176, -8.976)^T$  with corresponding 95% CI being  $(-5.353, 55.965)$  for the gradient measure and  $(-27.904, -0.073)$  for the curvature measure indicating that  $C$  forms a *curvature boundary*. Curves like  $C$  provide a deeper look into the tumor micro-environment.

## 7 Summary

We have developed an easy-to-use software for boundary analysis or, wombling under a Bayesian framework. We hope that it will find use in many applications, for example usage see [Banerjee and Gelfand \(2006\)](#); [Halder et al. \(2024a\)](#). The `sp_ggplot` function also features an option to supply shape-files for more mainstream geostatistical applications. Further examples are available on the GitHub repository: [arh926/nimblewomble/](https://github.com/arh926/nimblewomble/). Boundary analysis requires the investigator to pre-select curves. Identifying such curves in context of the application often proves crucial for detecting differential behavior in the response variable. `Nimble` facilitates an accessible MCMC framework that is immensely helpful in developing the statistical inference for rates of change and boundary analysis.

Future developments can proceed along many directions. We hope to expand the software to include spatiotemporal wombling (see, e.g., [Halder et al., 2024b](#)). Similar frameworks can be developed for generalized linear models, particularly focusing on zero-inflated models (see, e.g. [Finley et al., 2011](#); [Halder et al., 2021](#)) which provide a more realistic setting for analyzing raw gene-expression counts. We also plan to include code for inference on directional data considering Bayesian inference for the direction of maximum gradient and curvature (see, e.g., [Wang and Gelfand, 2014](#); [Wang et al., 2018](#)).

## 8 Supplement

**Theorem 1.** On each rectilinear segment,  $C_{t^*} = \{s_0 + tu : t \in [0, t^*]\}$ , where  $\mathbf{u}$  is a unit vector and  $\mathbf{u}^\perp$  is its normal, the terms in the cross-covariance matrix are

$$\begin{aligned} k_{ij}(t^*, t^*) &= (-1)^i \int_0^{t^*} \int_0^{t^*} \mathbf{a}_i(t_1)^\top \partial^{i+j} K(\Delta(t_1, t_2)) \mathbf{a}_j(t_2) \|\mathbf{s}'(t_1)\| \|\mathbf{s}'(t_2)\| dt_1 dt_2, \\ &= (-1)^i t^* \int_{-t^*}^{t^*} \mathbf{a}_i^\top \partial^{i+j} K(x\mathbf{u}) \mathbf{a}_j dx, \quad i, j = 1, 2, \end{aligned}$$

where  $\mathbf{a}_1(t) = \mathbf{n}(s(t))$  is the normal to the segment,  $\mathbf{a}_2(t) = \mathcal{E}_2 \mathbf{n}(s(t)) \otimes \mathbf{n}(s(t))$ , where  $\mathcal{E}_2 = \begin{pmatrix} 1 & \\ & 1 \end{pmatrix}$  is an elimination matrix and  $\Delta(t_1, t_2) = s_2(t) - s_1(t)$ .

*Proof.* Considering the parametric segment,  $C_{t^*} = \{s_0 + tu : t \in [0, t^*]\}$ , where  $\mathbf{u} = (u_1, u_2)^\top$  is a unit vector,  $\|\mathbf{u}\| = 1$ ,  $\mathbf{u}^\perp$  is its normal,  $\mathbf{u}^\top \mathbf{u}^\perp = 0$ ,  $\mathbf{a}_1(t) = \mathbf{a}_1 = \mathbf{u}^\perp$  and  $\mathbf{a}_2(t) = \mathbf{a}_2 = \mathcal{E}_2(\mathbf{u}^\perp \otimes \mathbf{u}^\perp)$  are free of  $t$ , and  $\Delta(t_1, t_2) = (t_2 - t_1)\mathbf{u}$ . The integrand in  $k_{ij}(t^*, t^*) = (-1)^i \int_0^{t^*} \int_0^{t^*} \mathbf{a}_i^\top \partial^{i+j} K((t_2 - t_1)\mathbf{u}) \mathbf{a}_j dt_1 dt_2$ , depends only on  $(t_2 - t_1)$ . Making a change of variable—define  $x = t_2 - t_1$ ,  $y = t_2 + t_1$ , implying  $\frac{x+y}{2} = t_2$  and  $\frac{y-x}{2} = t_1$ . The Jacobian is  $\frac{1}{2}$ . Hence,  $0 \leq y + x \leq 2t^*$  and  $0 \leq y - x \leq 2t^*$ . This implies  $0 \leq y \leq 2t^*$  and  $-t^* \leq x \leq t^*$ . Making the substitution above reduces,  $k_{ij}(t^*, t^*) = \frac{(-1)^i}{2} \int_0^{2t^*} \int_{-t^*}^{t^*} \mathbf{a}_i^\top \partial^{i+j} K(x\mathbf{u}) \mathbf{a}_j dx dy = (-1)^i t^* \int_{-t^*}^{t^*} \mathbf{a}_i^\top \partial^{i+j} K(x\mathbf{u}) \mathbf{a}_j dx$ . Setting  $i = j = 1$ , produces the scenario in [Banerjee and Gelfand \(2006\)](#).  $\square$

**Theorem 2.** For the Matérn kernel, with  $\nu = 3/2$ , the variance of the gradient based wombling measure is  $k_{11}(t^*, t^*) = 2\sqrt{3}\sigma^2\phi t^* G(1, \sqrt{3}\phi t^*)$ . In case  $\nu = 5/2$ , the cross-covariance matrix for the wombling measures based on spatial gradient and curvature requires  $k_{11}(t^*, t^*) = \frac{2\sqrt{5}}{3}\sigma^2\phi t^* \{G(1, \sqrt{5}\phi t^*) + G(2, \sqrt{5}\phi t^*)\}$ ,  $k_{22}(t^*, t^*) = 10\sqrt{5}\sigma^2\phi^3 t^* G(1, \sqrt{5}\phi t^*)$  and  $k_{21}(t^*, t^*) = -k_{12}(t^*, t^*) = 0$ , where  $G(a, \frac{x}{b}) = \int_0^{x/b} x^{a-1} e^{-x/b} dx$  is the lower incomplete Gamma function with shape parameter  $a$  and scale parameter  $b$ . For the Gaussian kernel,

$$\mathbf{V}_\Gamma(t^*) = 2\sigma^2 \sqrt{\pi}\phi t^* \{2\Phi(\sqrt{2}\phi t^*) - 1\} \begin{pmatrix} 1 & 0 \\ 0 & 6\phi^2 \end{pmatrix},$$

where  $\Phi(\cdot)$  is the cdf for the standard Gaussian probability density.

*Proof.* Using Theorem 1, if  $\nu = 3/2$ , then we obtain  $k_{11}(t^*, t^*) = 3\sigma^2\phi^2 t^* \int_{-t^*}^{t^*} e^{-\sqrt{3}\phi|x|} dx = 2\sqrt{3}\sigma^2\phi t^* G(1, \sqrt{3}\phi t^*)$ . If  $\nu = 5/2$ , then  $k_{11}(t^*, t^*) = \frac{5}{3}\sigma^2\phi t^* \int_{-t^*}^{t^*} (1 + \sqrt{5}\phi|x|) e^{-\sqrt{5}\phi|x|} dx = \frac{2\sqrt{5}}{3}\sigma^2\phi t^* \{G(1, \sqrt{5}\phi t^*) + G(2, \sqrt{5}\phi t^*)\}$ . For terms  $k_{21}$  and  $k_{12}$ , let us consider  $\mathbf{a}_1^\top \partial^3 K(x\mathbf{u}) \mathbf{a}_2 = \frac{25}{3}\sigma^2\phi e^{-\sqrt{5}\phi|x|} |\mathbf{a}_1^\top \mathbf{A}_1 \mathbf{a}_2 - \sqrt{5}\phi|x| \mathbf{a}_1^\top \mathbf{A}_2 \mathbf{a}_2|$ , where

$$\mathbf{A}_1 = \begin{pmatrix} 3u_1 & u_2 & u_1 \\ u_2 & u_1 & 3u_2 \end{pmatrix}, \quad \mathbf{A}_2 = \begin{pmatrix} u_1^3 & u_1^2 u_2 & u_2^2 u_1 \\ u_1^2 u_2 & u_2^2 u_1 & u_2^3 \end{pmatrix}.$$

The first and the second term both reduce to 0. Hence,  $k_{21}(t^*, t^*) = -k_{12}(t^*, t^*) = 0$ . Next,  $a_2^\top \partial^4 K(xu) a_2 = \frac{25}{3} \sigma^2 \phi^4 e^{-\sqrt{5}\phi|x|} \{a_2^\top A_3 a_2 - \sqrt{5}\phi|x| a_2^\top A_4 (\sqrt{5}\phi|x| + 1) a_2\}$ , where

$$A_3 = \begin{pmatrix} 3 & 0 & 1 \\ 0 & 1 & 0 \\ 1 & 0 & 3 \end{pmatrix}, \quad A_4(x') = \begin{pmatrix} 6u_1^2 - x' u_1^4 & (3-x' u_1^2) u_1 u_2 & 1-x' u_1^2 u_2^2 \\ (3-x' u_1^2) u_1 u_2 & 1-x' u_1^2 u_2^2 & (3-x' u_2^2) u_1 u_2 \\ 1-x' u_1^2 u_2^2 & (3-x' u_2^2) u_1 u_2 & 6u_2^2 - x' u_2^4 \end{pmatrix}.$$

After some algebra,  $a_2^\top \partial^4 K(xu) a_2 = 25\sigma^2 \phi^4 e^{-\sqrt{5}\phi|x|} \{1 - 2\sqrt{5}\phi|x| u_1^\perp u_2^\perp (u_1 u_2 + u_1^\perp u_2^\perp)\}$ . Observe that  $u_1^\perp = u_2$  and  $u_2^\perp = -u_1$ , substituting we get  $k_{22}(t^*, t^*) = 10\sqrt{5}\sigma^2 \phi^3 t^* G(1, \sqrt{5}\phi t^*)$ .

For the Gaussian kernel,  $k_{11}(t^*, t^*) = 2\sigma^2 \phi^2 t^* \int_{-t^*}^{t^*} e^{-\phi^2 x^2} dx = 2\sigma^2 \sqrt{\pi} \phi t^* \{2\Phi(\sqrt{2}\phi t^*) - 1\}$ . Note that  $a_1^\top \partial^3 K(xu) a_2 = 4\sigma^2 \phi^4 e^{-\phi^2 x^2} x \{a_1^\top A_1 a_2 - 2\phi^2 x^2 a_1^\top A_2 a_2\}$ . Again, the first and second terms equate to 0 implying  $k_{21}(t^*, t^*) = -k_{12}(t^*, t^*) = 0$ . Next,  $a_2^\top \partial^4 K(xu) a_2 = 4\sigma^2 \phi^4 e^{-\phi^2 x^2} \{a_2^\top A_3 a_2 - 2\phi^2 x^2 a_2^\top A_4 (2\phi^2 x^2) a_2\}$ . After some algebra,  $a_2^\top \partial^4 K(xu) a_2 = 12\sigma^2 \phi^4 e^{-\phi^2 x^2} \{1 - 4\phi^2 x^2 u_1^\perp u_2^\perp (u_1 u_2 + u_1^\perp u_2^\perp)\}$ . Substituting, we get  $k_{22}(t^*, t^*) = 12\sigma^2 \sqrt{\pi} \phi^3 t^* \{2\Phi(\sqrt{2}\phi t^*) - 1\}$  resulting in the required expression for  $V_\Gamma(t^*)$ .  $\square$

Theorem 2 interestingly shows that the posited cross-covariance matrix,  $V_\Gamma(t^*)$ , reduces to a *variance-covariance matrix*. It has a simpler form for the Gaussian case when compared to Matérn with  $\nu = \frac{5}{2}$ . Finally, considering the covariance between  $Z(s_i)$ ,  $i = 1, \dots, N$  and the wombling measures—in the Gaussian case, closed-forms are available (see, e.g., Halder et al., 2024a, end of Section 3). The inferential exercise of wombling does not require quadrature when using a Gaussian kernel however, only one-dimensional quadrature is required for the same when using a Matérn kernel.

## Bibliography

- M. Abramowitz, I. A. Stegun, and R. H. Romer. Handbook Of Mathematical Functions With Formulas, Graphs, and Mathematical Tables, 1988. [p1, 3]
- S. Banerjee. Spatial gradients and wombling. In *Handbook of Spatial Statistics*, pages 559–575. Taylor & Francis, 08 2010. ISBN 978-1-4200-7287-7. doi: 10.1201/9781420072884-c31. [p1]
- S. Banerjee and A. E. Gelfand. On smoothness properties of spatial processes. *Journal of Multivariate Analysis*, 84(1):85–100, Jan. 2003. ISSN 0047-259X. [p2]
- S. Banerjee and A. E. Gelfand. Bayesian Wombling: Curvilinear Gradient Assessment Under Spatial Process Models. *Journal of the American Statistical Association*, 101(476):1487–1501, 2006. [p1, 4, 11]
- S. Banerjee, A. E. Gelfand, and C. F. Sirmans. Directional Rates of Change Under Spatial Process Models. *Journal of the American Statistical Association*, 98(464):946–954, Dec. 2003. ISSN 0162-1459. [p1, 2]
- S. Banerjee, B. P. Carlin, and A. E. Gelfand. *Hierarchical Modeling and Analysis for Spatial Data*. Chapman and Hall/CRC, New York, 2 edition, Sept. 2014. ISBN 978-0-429-13717-4. [p1]
- J. Chen, C. Xiong, Q. Sun, G. W. Wang, G. P. Gupta, A. Halder, Y. Li, and D. Li. Investigating spatial dynamics in spatial omics data with StarTrail, May 2024. [p10]
- P. de Valpine, D. Turek, C. J. Paciorek, C. Anderson-Bergman, D. T. Lang, and R. Bodik. Programming With Models: Writing Statistical Algorithms for General Model Structures With NIMBLE. *Journal of Computational and Graphical Statistics*, 26(2):403–413, Apr. 2017. ISSN 1061-8600. [p1]
- A. O. Finley. *MBA: Multilevel B-Spline Approximation*, 2024. R package version 0.1-2. [p2]
- A. O. Finley, S. Banerjee, and B. P. Carlin. spBayes: An R Package for Univariate and Multivariate Hierarchical Point-referenced Spatial Models. *Journal of Statistical Software*, 19:1–24, Apr. 2007. ISSN 1548-7660. [p1]
- A. O. Finley, S. Banerjee, and D. W. MacFarlane. A Hierarchical Model for Quantifying Forest Variables Over Large Heterogeneous Landscapes With Uncertain Forest Areas. *Journal of the American Statistical Association*, 106(493):31–48, Mar. 2011. ISSN 0162-1459. [p11]
- A. O. Finley, A. Datta, B. D. Cook, D. C. Morton, H. E. Andersen, and S. Banerjee. Efficient Algorithms for Bayesian Nearest Neighbor Gaussian processes. *Journal of Computational and Graphical Statistics*, 28(2):401–414, 2019. [p4]

- L. Gao, S. Banerjee, and B. Ritz. Spatial Difference Boundary Detection for Multiple Outcomes Using Bayesian Disease Mapping. *Biostatistics*, 24(4):922–944, Oct. 2023. ISSN 1465-4644. [p1]
- J. F. Gleyze, J. N. Bacro, and D. Allard. Detecting regions of abrupt change: Wombling procedure and statistical significance. In P. Monestiez, D. Allard, and R. Froidevaux, editors, *geoENV III — Geostatistics For Environmental Applications*, pages 311–322, Dordrecht, 2001. Springer Netherlands. ISBN 978-94-010-0810-5. [p1]
- B. Goldstein and P. de Valpine. Comparing N-mixture models and GLMMs for relative abundance estimation in a citizen science dataset. *Scientific Reports*, 12:12276, 2022. [p1]
- B. R. Goldstein, D. Turek, L. Ponisio, and P. de Valpine. nimbleEcology: Distributions for ecological models in nimble, 2024. URL <https://cran.r-project.org/package=nimbleEcology>. R package version 0.5.0. [p1]
- A. Halder, S. Mohammed, K. Chen, and D. K. Dey. Spatial Tweedie Exponential Dispersion Models: An Application to Insurance Rate-Making. *Scandinavian Actuarial Journal*, 2021(10):1017–1036, 2021. [p11]
- A. Halder, S. Banerjee, and D. K. Dey. Bayesian Modeling with Spatial Curvature Processes. *Journal of the American Statistical Association*, 119(546):1155–1167, Apr. 2024a. ISSN 0162-1459. [p1, 2, 4, 11, 12]
- A. Halder, D. Li, and S. Banerjee. Bayesian Spatiotemporal Wombling. *arXiv preprint arXiv:2407.17804*, 2024b. [p11]
- A. L. Ji, A. J. Rubin, K. Thrane, S. Jiang, D. L. Reynolds, R. M. Meyers, M. G. Guo, B. M. George, A. Mollbrink, J. Bergensträhle, L. Larsson, Y. Bai, B. Zhu, A. Bhaduri, J. M. Meyers, X. Rovira-Clavé, S. T. Hollmig, S. Z. Aasi, G. P. Nolan, J. Lundeberg, and P. A. Khavari. Multimodal Analysis of Composition and Spatial Architecture in Human Squamous Cell Carcinoma. *Cell*, 182(2):497–514.e22, July 2020. ISSN 1097-4172. [p9]
- J. T. Kent. Continuity Properties for Random Fields. *The Annals of Probability*, 17(4):1432–1440, 1989. ISSN 0091-1798. Publisher: Institute of Mathematical Statistics. [p1]
- F. Lindgren and H. Rue. Bayesian Spatial Modelling with R-INLA. *Journal of Statistical Software*, 63: 1–25, Feb. 2015. ISSN 1548-7660. [p1]
- L. Ponisio, P. de Valpine, N. Michaud, and D. Turek. One size does not fit all: Customizing mcmc methods for hierarchical models using NIMBLE. *Ecology and Evolution*, 10:2385–2416, 2020. [p1]
- K. Qu, B. , Jonathan R. , and X. Niu. Boundary Detection Using a Bayesian Hierarchical Model for Multiscale Spatial Data. *Technometrics*, 63(1):64–76, Jan. 2021. ISSN 0040-1706. [p1]
- R Core Team. *R: A Language and Environment for Statistical Computing*. R Foundation for Statistical Computing, Vienna, Austria, 2021. [p1]
- C. E. Rasmussen and C. K. I. Williams. *Gaussian Processes for Machine Learning*. The MIT Press, Nov. 2005. ISBN 978-0-262-25683-4. [p1]
- M. D. Risser and D. Turek. Bayesian inference for high-dimensional nonstationary Gaussian processes. *Journal of Statistical Computation and Simulation*, 90(16):2902–2928, Nov. 2020. ISSN 0094-9655. [p1]
- M. L. Stein. *Interpolation of Spatial Data*. Springer Series in Statistics. Springer, New York, NY, 1999. [p2]
- S. Sun, J. Zhu, and X. Zhou. Statistical analysis of spatial expression patterns for spatially resolved transcriptomic studies. *Nature Methods*, 17(2):193–200, Feb. 2020. ISSN 1548-7105. Publisher: Nature Publishing Group. [p10]
- V. Svensson, S. A. Teichmann, and O. Stegle. SpatialDE: identification of spatially variable genes. *Nature Methods*, 15(5):343–346, May 2018. ISSN 1548-7105. Publisher: Nature Publishing Group. [p10]
- D. Turek, P. de Valpine, and C. Paciorek. Efficient markov chain monte carlo sampling for hierarchical hidden markov models. *Environmental and Ecological Statistics*, 23:549–564, 2016. [p1]
- F. Wang and A. E. Gelfand. Modeling Space and Space-Time Directional Data Using Projected Gaussian Processes. *Journal of the American Statistical Association*, 109(508):1565–1580, 2014. [p11]
- F. Wang, A. Bhattacharya, and A. E. Gelfand. Process modeling for slope and aspect with application to elevation data maps. *TEST*, 27(4):749–772, Dec. 2018. ISSN 1863-8260. [p11]

- L. M. Weber, A. Saha, A. Datta, K. D. Hansen, and S. C. Hicks. nnSVG for the scalable identification of spatially variable genes using nearest-neighbor Gaussian processes. *Nature Communications*, 14(1):4059, July 2023. ISSN 2041-1723. Publisher: Nature Publishing Group. [p10]
- H. Wickham. ggplot2. *Wiley interdisciplinary reviews: computational statistics*, 3(2):180–185, 2011. [p2]
- W. H. Womble. Differential Systematics. *Science*, 114(2961):315–322, Sept. 1951. Publisher: American Association for the Advancement of Science. [p1]
- K. L. Wu and S. Banerjee. Assessing Spatial Disparities: A Bayesian Linear Regression Approach, Mar. 2025. [p1]

*Aritra Halder*

*Department of Biostatistics & Epidemiology*  
3215 Market Street, Philadelphia, PA 19104  
<https://orcid.org/0000-0002-5139-3620>  
[aritra.halder@drexel.edu](mailto:aritra.halder@drexel.edu)

*Sudipto Banerjee*

*Department of Biostatistics*  
*University of California, Los Angeles*  
650 Charles E. Young Drive South, Los Angeles, CA 90095  
<https://orcid.org/0000-0002-2239-208X>  
[sudipto@ucla.edu](mailto:sudipto@ucla.edu)